5 Depth Perception: Quantifying Cellular Traction Forces in Three Dimensions

The work presented here is taken from:

*Maskarinec, S.A., *Franck C., Tirrell, D.A., and G. Ravichandran. *Depth Perception: Quantifying Cellular Traction Forces in Three Dimensions*, submitted for publication.

*Signifies equal contributions

5.1 Abstract

Cells engage in mechanical force exchange with their extracellular environment through tension generated by the cytoskeleton. A new method, combining laser scanning confocal microscopy (LSCM) and digital volume correlation (DVC), enables tracking and quantification of cell-mediated deformation of the extracellular matrix in all three spatial dimensions. Time-lapse confocal imaging of migrating 3T3 fibroblasts on fibronectin (FN)-modified polyacrylamide gels of varying thickness reveals significant in-plane (x, y) and normal (z) displacements, and illustrates the extent to which cells, even in nominally two-dimensional environments, explore their surroundings in all three dimensions. The magnitudes of the measured displacements are independent of the elastic moduli of the gels. Analysis of the normal displacement profiles suggests that normal forces play important roles even in two-dimensional cell migration.

5.2 Introduction

The measurement of cellular traction forces has been of increasing interest since the discovery that the mechanical properties of the cellular microenvironment can direct many important cellular processes including spreading, migration, and differentiation [1-4]. It is now widely accepted that mechanical properties must be considered along with chemical signals if we are to understand how cells integrate environmental cues to modulate their behavior [5-8]. The correlation between cell-induced deformations in materials and biochemical signaling and regulation, particularly focal adhesion formation and clustering, has been investigated through the use of a variety of techniques including surface wrinkling, displacement-tracking using traction force microscopy (TFM), and bending of pillar arrays [9-15]. These methods have yielded substantial insight into cellular behavior, but are inherently restricted to two-dimensional (2-D) analysis and interpretation of cell-matrix interactions. Furthermore, these approaches calculate stresses by comparing images before and after cell detachment [10], thus providing only snapshots of cell behavior rather than dynamic analyses of the processes by which cells explore their microenvironments.

In this report, we demonstrate the capability to dynamically track and quantify cellular traction forces in three dimensions (3-D). Mechanical interactions between 3T3 fibroblasts and FN-modified polyacrylamide gels are quantified dynamically by computing the displacement and traction fields generated by motile cells. Use of a recently developed digital volume correlation (DVC) method [16] allows three-dimensional displacements and traction fields to be determined directly from volumetric confocal image stacks, and obviates the need for complex inverse formulations [10]. The

method has a temporal resolution that permits confocal imaging over time scales relevant for the migration of anchorage-dependent cells such as endothelial cells and fibroblasts [17].

The 3-D character of this approach relies on the use of laser scanning confocal microscopy (LSCM), which has the distinct advantage over conventional microscopic imaging in that it provides positional information along the z-axis, i.e, in the direction normal to the plane of the sample [18]. A schematic of the experimental setup is shown in Figure 5-1 (A). The range of gel thicknesses investigated was between 20–100 μm, and the height contribution of the covalently attached FN layer measured by confocal scanning was less than 1 μm. Samples were produced with two different crosslink densities to achieve physiologically relevant values of the elastic modulus (E, 0.82 (± 0.23) kPa and 9.64 (± 1.12) kPa) [19]. Red fluorescent microspheres (0.5 μm in diameter) were embedded during gel formation to enable tracking of cell-generated deformations by DVC. Simultaneous visualization of the red fluorescent markers and the cell was accomplished by allocating separate lasers and filters along with the use of a 3T3 fibroblast cell line transfected with a vector encoding a green fluorescent protein (GFP)-actin fusion construct. Cells were deposited on the surfaces of the FN-modified samples and incubated overnight to ensure attachment before imaging. Isolated cells were imaged every 35 minutes for up to 24 hours within a typical field of view of 150 x 150 x 150 μm^3. Figure 5-1 (B) shows a cross-sectional view of a typical confocal stack. Imaging of isolated cells ensures that neighboring cells do not contribute to the measured displacements.

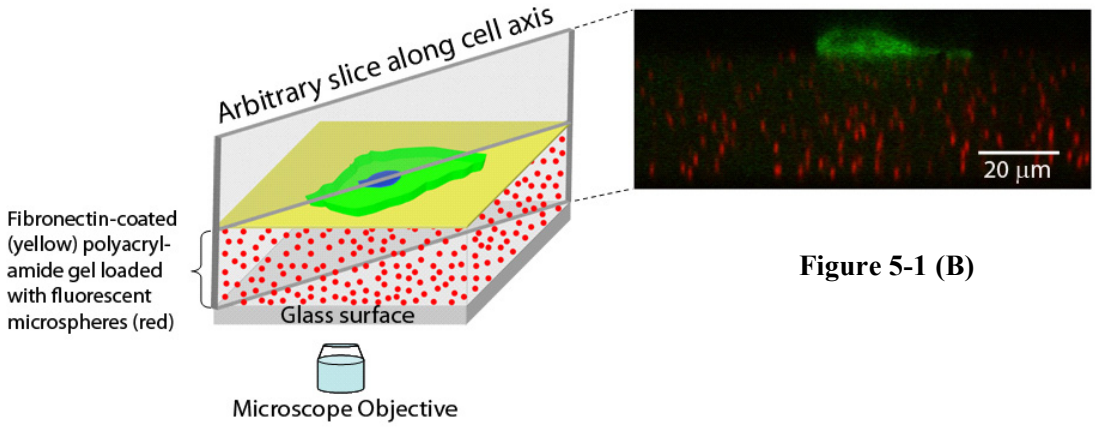

Figure 5-1 (A)

Figure 5-1 (B)

Figure 5-1. (A) Schematic of a representative gel sample with microscope objective. 3-D confocal image stacks are acquired every 35 minutes through an inverted microscope that captures the emission from both the fluorescent microspheres (red) and GFP-transfected cells (green). The 35-minute time interval was chosen for investigating fibroblast migration patterns given measured migration speeds of ~ 8 μm/hour, as well as to minimize phototoxicity to cells. (B) Cross-sectional view of a typical confocal image stack. Cells migrate on the surface of the FN-modified polyacrylamide gel, and the corresponding displacements in the underlying gel are monitored. The red fluorescent microspheres are visible within the gel.

As the cell explores the substrate and probes its resistance to deformation, displacements are determined by comparing successive stacks. Most importantly, the DVC method can map such displacements in all three dimensions by comparing uniquely defined cubic subsets within confocal stacks that are obtained sequentially [16]. This technique can detect both translational and rotational changes, and is valid for large deformations. The technique is sensitive to displacement changes greater than or equal to

0.12 μm with a spatial resolution of approximately 2 μm, and can reach finer (submicron) spatial resolution at a greater computational cost.

5.3 Materials and Methods

5.3.1 Preparation of activated coverslips

Glass coverslips (Gold-Seal coverslip No 0, Electron Microscopy Sciences, Hatfield, PA) were chemically modified to allow covalent attachment of polyacrylamide films using previously established protocols with some modifications [10, 20]. Briefly, coverslips were rinsed with ethanol before being placed in a dish containing a solution of 0.5% (v/v) 3-aminopropyltrimethoxysilane (Gelest, Inc., Morrisville, PA) in ethanol for 5 minutes. The coverslips were removed from the dish and rinsed with a stream of ethanol before being immediately placed treated-side up in a solution of 0.1% (v/v) glutaraldehyde (Polysciences, Inc., Warrington, PA) in water for 30 minutes. Activated coverslips were rinsed with a stream of deionized water and left to dry for several hours at 60^{o}C. Treated coverslips were covered and stored for up to one week after preparation.

5.3.2 Preparation of polyacrylamide films

Thin films of polyacrylamide were generated and fused to functionalized coverslips using a protocol adopted from previous reports with some modifications [10, 20]. Solutions of acrylamide (40% w/v, Bio-Rad, Hercules, CA) and N, N-methylene-bis-acrylamide (BIS, 2.5% w/v, Bio-Rad, Hercules, CA) were mixed with distilled water to obtain the following concentrations used for tested samples: 1) 10% acrylamide and 0.015% BIS, and 2) 10% acrylamide and 0.0075% BIS. Adjusting the concentration of

BIS in the formulation was used to create substrates with varying mechanical properties. To these solutions, red fluorescent microparticles (0.5 μm, carboxylate-modified, Molecular Probes, Carlsbad, CA) were vortexed for 10 seconds and subsequently added in a volume ratio of 9:100. Crosslinking was initiated through the addition of ammonium persulfate (Sigma-Aldrich, St. Louis, MO) and N, N, N',N'-tetramethyl-ethylenediamine (Invitrogen, Carlsbad, CA). The samples were vortexed for 10 seconds, and 5–7 microliters of the acrylamide solution was pipetted on the surface of a precleaned microscope slide (No. 1, 75 mm x 25 mm, Corning, Corning, NY). To generate thicker films, 20–40 microliters of the solution was used. The activated surface of the coverslip was then placed on top of the acrylamide droplet, causing the solution to flatten under the weight of the coverslip. The entire assembly was left undisturbed for 5 minutes, and then placed in a Petri dish (100 mm diameter, VWR, West Chester, PA) containing distilled water for 10–30 minutes. The bonded sample was then peeled from the microscope slide using forceps and thoroughly rinsed with several volume changes of water.

5.3.3 Functionalization of polyacrylamide films with fibronectin

In order to promote cell attachment to polyacrylamide films, a saturating density of fibronectin was conjugated to the gel surface using the heterobifunctional crosslinker, sulfo-SANPAH (Pierce Chemicals, Rockford, IL). Adopting procedures outlined previously [10, 20], polyacrylamide gel samples were briefly dried in air to rid the surface of excess water before 200 μl of sulfo-SANPAH in water (1.0 mg/ml) was applied. The surface of the sample was then exposed to unfiltered UV light from a high-pressure mercury lamp (Oriel Q 100W at 5 A, > 10 min warm up time) at a distance of 10

inches for 7.5 minutes. The darkened sulfo-SANPAH solution was removed from the surface of the gel and replaced with another 200 μl aliquot and irradiated for another 7.5 minutes for a total of 15 minutes of UV exposure. The samples were then rinsed vigorously with water for 5 minutes, and adhered to the bottom of 60 mm Petri dishes (Becton Dickinson, Franklin Lakes, NJ) by applying a thin layer of vacuum grease (Dow Corning, Midland, MI) around the perimeter of the unmodified side of the coverslip. The samples were rinsed twice with phosphate buffered saline (PBS, pH 7.4), covered with a solution of fibronectin (FN, 0.2 mg/ml, Millipore, Billerica, MA) and left undisturbed overnight at 4^{o}C. Following overnight incubation, the substrates were rinsed three times with PBS.

5.3.4 Characterization of FN-modified films

Comparison of the relative amounts of covalently attached FN on polyacrylamide (PA) samples made with varying percentages of crosslinker was conducted using a commercially available bicinchoninic acid (BCA) assay kit (Sigma-Aldrich, St. Louis, MO). In this assay, the relative protein concentration is quantified by measuring the absorbance at 562 nm using a plate reader and comparing the measured values to a standard curve generated using known amounts of FN (Tecan Sapphire, Tecan Group Ltd., Männedorf, Switzerland). A set of FN-modified samples (lacking embedded microspheres) was prepared as described above and placed in a 6-well plate (Becton Dickinson, Franklin Lakes, NJ). Negative controls consisting of unmodified samples made with similar crosslinker percentages (% BIS) were also prepared. All samples were

then treated for 1 hour at 60^{o}C followed by an absorbance reading. These experiments were repeated three times in triplicate for each % BIS.

5.3.5 Film thickness measurements

The thickness of the sample was determined by calculating the distance from the bottom of the glass surface to the disappearance of bead fluorescence at the top of the sample using a confocal microscope. The sample thicknesses were controlled by adjusting the total volume of the acrylamide mixture used to make the samples.

5.3.6 Mechanical characterization of thin films

The mechanical properties of the substrates were determined by performing both unconfined and confined compression testing on cylindrical polyacrylamide specimens using a custom-built compression setup ([16], Figure 5-2). The typical sample dimensions were 8 mm in diameter and 4 mm in height. The displacements during each compression increment were controlled using a digital micrometer with a resolution of 1 μm. The resulting nominal force was measured using a 10 g load cell (A.L. Design, Buffalo, NY). For each volume fraction of BIS crosslinker used, 6–8 samples were tested in both confined and unconfined uniaxial compression.

For unconfined tests, gel samples were cast in a circular washer secured to the bottom of a 60 mm diameter plastic Petri dish. Following polymerization (~ 2–5 minutes), the washer was removed from the dish and the sample was hydrated and left covered at room temperature overnight to ensure adequate swelling. Prior to compression, the alignment of the setup with the sample was inspected to ensure pure

compression along the nominal loading axis. The samples were compressed between the top platen of the compression setup and the bottom of the Petri dish with a nominal strain increment of 1–2%. Nominal strain increments are defined by the ratio of the displacement increment resulting from the compression to the original sample height. Force values were obtained continuously during each 5-minute increment in order to detect any time-dependent relaxation of the material during the compression. The total applied nominal compressive strain was ~ 13–15%. After complete loading, the sample was successively unloaded using the same strain increments to record the entire loading-unloading cycle.

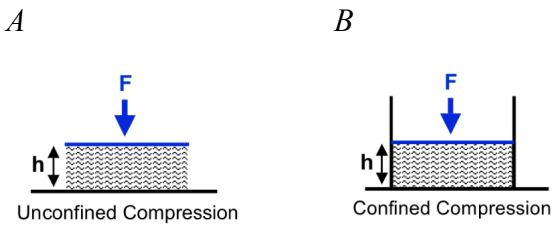

Figure 5-2. Detailed schematic of the compression tests: (A) Unconfined compression tests, (B) Confined compression tests.

5.3.7 Cell culture

Prior to depositing cells, FN-modified gel samples were equilibrated in growth media at 37^{o}C for 15 minutes. Swiss 3T3 fibroblasts transfected with a GFP-actin vector (a gift from Professor Scott Fraser, California Institute of Technology) were cultured in Dulbecco's Modified Eagle Medium (DMEM) supplemented with 10% fetal bovine serum, 50 ug/ml streptomycin, and 50 U/ml penicillin (Invitrogen, Carlsbad, CA). For all experiments, cells were first treated with Mitotracker Deep Red (Molecular Probes, Carlsbad, CA) for 45 minutes before passaging with trypsin-EDTA (0.05%, Invitrogen,

Carlsbad, CA). Mitotracker dyes accumulate in actively respiring mitochondria providing a second method for tracking cells and determining cell viability. Cells were plated at density of ~ 40,000 cells/coverslip, and incubated on samples for 8–12 hours before imaging.

5.3.8 Confocal microscopy and time-lapse imaging

3-D image stacks were acquired using a Nikon C-1 confocal system mounted on a TE-2000-U inverted optical microscope. A 40x CFI planar fluor air objective with a numerical aperture of 0.6 was used in all experiments. Three laser lines were used to image the cells and the fluorescent microparticles: Argon (488 nm) laser for the GFP-actin, a green HeNe (543 nm) for the microparticles in the polyacrylamide gels, and a red HeNe (633 nm) for the Mitotracker Deep Red for mitochondrial labeling. Confocal stacks were acquired every 35 minutes for several hours at a resolution of 512 x 512 x H (X *x* Y *x* Z) pixels^3, where H ranges from 120–250 pixels. Typical imaging areas were between 150–200 μm^2; images with a larger field of view were captured before and after experiments to ensure that measured displacements were not the result of contributions from neighboring cells. Physiological conditions were maintained during all times by housing the entire confocal microscope inside a custom-built temperature controlled chamber. The temperature was controlled using a feedback controlled heater, Air-Therm ATX Air Heater Controller (World Precision Instruments, Sarasota, FL), and an arterial blood gas mixture (5% CO_2, 20% O_2, 75% N_2) was injected into the chamber in order to maintain appropriate culturing conditions.

5.3.9 Calculation of displacements, strains, stresses, and forces

The full-field 3-D displacements are determined using LSCM and DVC as previously described [16]. In brief, a digital volume cross-correlation algorithm is used to determine the 3-D cell-induced displacement fields from confocal volume stacks during each time increment. Once the entire displacement field is determined, the strain tensor of the material substrate is computed using a displacement-gradient technique [16]. The material stress tensor $\boldsymbol{\sigma}$ is then determined through the materials' constitutive relations, which were determined from the above characterization tests describing the material as a linearly elastic, isotropic, incompressible material. Hence, $\boldsymbol{\sigma}$ is calculated as $\boldsymbol{\sigma} = 2\mu\boldsymbol{\varepsilon}$, where $\boldsymbol{\varepsilon}$ is the computed strain tensor, and μ is the shear modulus and is related to Young's modulus by $E = \mu / (1 + \nu)$, with $\nu = 0.5$.

Traction forces are calculated along the top surface plane, directly beneath the cell using the known Cauchy relationship: $\mathbf{T} = \boldsymbol{\sigma}\mathbf{n}$, where $\mathbf{T}$ is the 3-D surface traction vector, $\boldsymbol{\sigma}$ is the material stress tensor, and $\mathbf{n}$ is the surface normal.

In order to establish the maximum resolution of the DVC-LSCM technique for the presented results here, several sets of confocal images of FN-modified polyacrylamide substrate samples were obtained under zero-load conditions at physiological conditions as described above. The computed uncertainties in the displacement measurements were found to be close to the previously published uncertainties [16], establishing subpixel or submicron resolution.

5.3.10 Traction force inhibition using blebbistatin

Time-lapse imaging of fibroblasts treated with the myosin-II-specific blocker, blebbistatin (Sigma-Aldrich, St. Louis, MO), were performed to establish that measured displacement were indeed cell-mediated and not the result of thermal fluctuations within the polyacrylamide sample. Blebbistatin is commonly used in traction force measurements to inhibit actinomyosin contraction in non-muscle cells [21, 22]. Confocal stacks of individual cells were captured 1–2 hours before treatment with 12.5 μM blebbistatin in dimethyl sulfoxide, and up to 4 hours post-treatment. Identical experiments were performed without cells and in the presence of blebbistatin.

5.4 Results and Discussion

5.4.1 Characterization of FN-modified films

The protein content for both sets of samples were similar (91.6 ± 52.4 μg for 0.015% BIS, and 82.7 ± 48.7 μg for 0.0075% BIS), and lie within the standard deviation calculated from the tested samples. These results confirm that the prepared samples display similar amounts of FN on the surface, and that changes in cell behavior result from differences in mechanical properties and not some difference in the chemical composition of the surfaces.

5.4.2 Mechanical Testing

Figure 5-3 shows the raw data for an incremental loading cycle highlighting negligible time-dependent behavior of the polyacrylamide samples, and Figure 5-4 shows the loading-unloading stress strain curve for a typical sample. The Young's modulus for

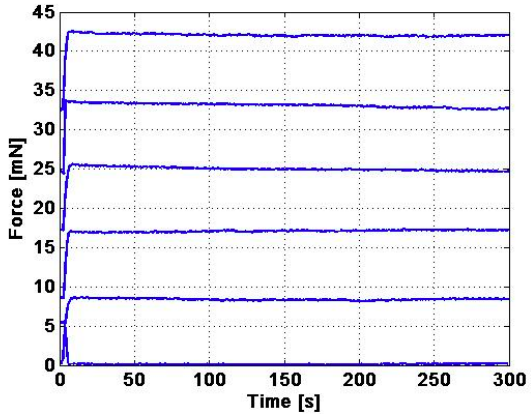

Figure 5-3. Incremental loading tests using polyacrylamide samples highlighting the negligible time-dependent relaxation behavior of the material. Force values were obtained continuously during 5-minute increments.

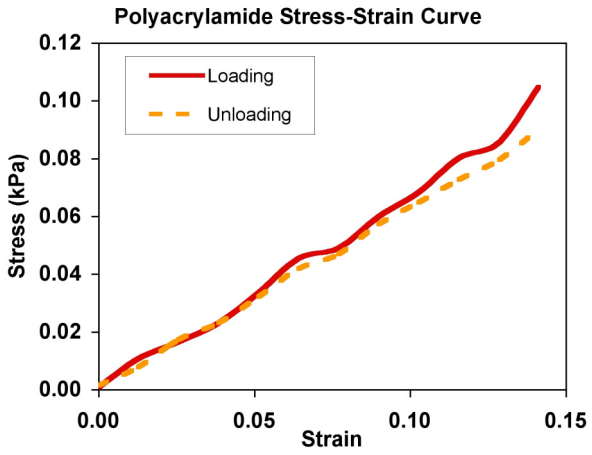

Figure 5-4. Representative stress-strain curves of loading and unloading cycles on cylindrical hydrated polyacrylamide samples demonstrating a linear elastic material response with negligible hysteresis.

the polyacrylamide samples was calculated from each stress-strain curve using the relationship:

$$E = \frac{\sigma}{\varepsilon} = \frac{F/A}{\Delta h/h}$$

where σ and ε denote the uniaxial stress and strain, and can be expressed as the applied force per sample contact area, and change in sample height over its original height. Table 5-1 summarizes the unconfined compression test results for two different crosslinker volume fractions.

Table 5-1. Mechanical characterization results for polyacrylamide substrates from unconfined uniaxial compression experiments.

Crosslinker Volume Fraction	**Young's Modulus (kPa)**
0.015% BIS	9.64 ± 1.12
0.0075% BIS	0.82 ± 0.23

In order to determine Poisson's ratio for each polyacrylamide gel, cylindrical specimens were cast and polymerized in a confined Teflon sleeve 15 mm in diameter and about 8 mm in height. Samples were hydrated following the same protocol as described above. The samples were compressed following the same loading-unloading protocol as for the unconfined test. Using the determined Young's modulus value of the unconfined test case and observing that the further compression beyond an initial compression strain of ~ 0.25% was not possible (due to the Poisson effect), Poisson's ratio was determined to be ~ 0.48–0.5 according to the following equation:

$$\overline{E} = \frac{\sigma}{\varepsilon} = \frac{1-\upsilon}{(1+\upsilon)(1-2\upsilon)}E$$

where $\bar{E}$ denotes the measured confined compression modulus, ν is the Poisson's ratio, and E is the Young's modulus as determined from unconfined compression test. From this set of experiments, Poisson's ratio was taken to be 0.5, and the material behavior is described as a linearly elastic, isotropic, and incompressible for all traction force calculations.

5.4.3 Analysis of cellular traction forces in 3D: in-plane and normal components

Detection of both normal and in-plane displacements allows a more complete analysis of cellular forces than does consideration of only in-plane (2-D) displacements [10]. Figure 5-5 shows the extent of cell-induced deformation as a function of depth within each substrate, and shows clearly that the z-axis displacement can be comparable to, or greater than, the in-plane displacement. In the images in Figure 5-5 (A), a slice along the long axis of the cell is shown, and the cell has been rendered in 3-D and superimposed to correlate its position with the observed displacements. The colored displacement contours show that larger displacements are concentrated near the top surface of the gel, and that these displacements decay from the top surface through the depth. Comparing the displacement patterns on gels of varying thicknesses, we find that displacements are more localized near the cell body on thinner samples (20 μm), and decay more gradually in thicker samples (80 μm). The decay profiles of individual displacement components as well as the total displacements for substrates of varying thicknesses are displayed as line plots in Figure 5-5 (B). All plots were generated by selecting one position along the thickness cross section of the sample near the leading edge of the migrating cell. This position corresponds to the region of maximum

deformation at a given time point. Displacement decays are also notable in the x-y displacements as a function of distance from the cell, and in some cases, drop off more steeply than the z-component. The total displacement profile at a given time point and slice location can be dominated by either in-plane or normal displacements, demonstrating how force-mediated deformations fluctuate during cell movement. Analysis of the ratios of the magnitudes of the individual components of the 3D displacement vector to the magnitude of the vector itself showed similar values for all three components ($\overline{x} = 0.58 \pm 0.29$, $\overline{y} = 0.43 \pm 0.23$, $\overline{z} = 0.50 \pm 0.32$, for N = 38 samples), further demonstrating the importance of measuring displacements in all three dimensions.

It is worth noting that deformation of the substrate can be detected at substantial depths below the top surface of each sample, and that this effect can be especially important for thin gels. For example, the fact that measurable displacements extend throughout more than half the thickness of the 20 μm sample, illustrates the importance of considering film thickness in designing experiments to monitor cellular response. In particular, if the substrate thickness is comparable to the extent of the deformation field, a cell seeded on a soft substrate that is bonded to a substantially stiffer support (e.g., glass), may be able to sense the mechanical constraint of the underlying plate. For the samples shown in Figure 5-5, the maximum extent of deformation as a fraction of the sample thickness decreased from 67% to 23% as the gel thickness increased from 20 to 80 μm.

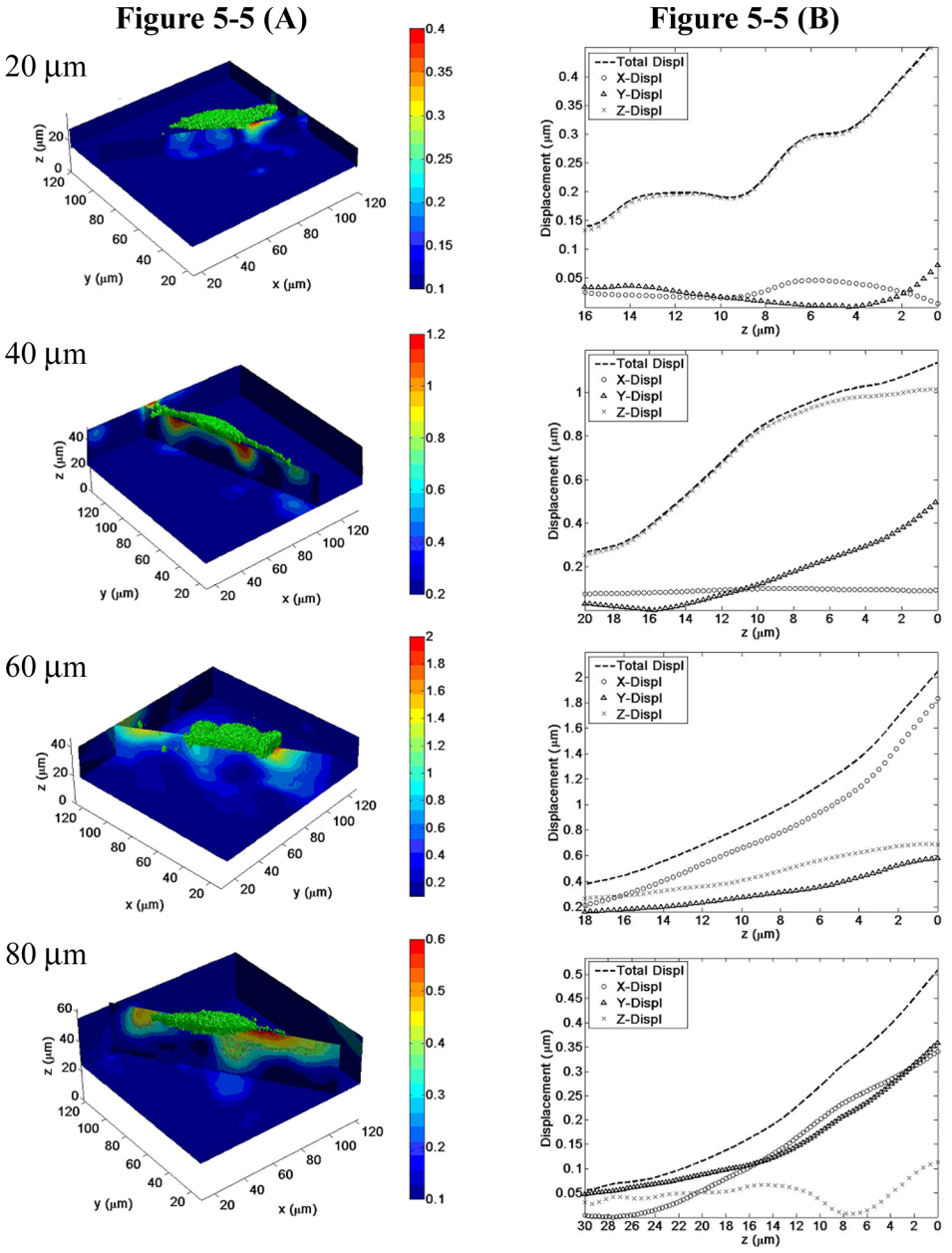

Figure 5-5. Displacement contour slices along the long axis of the cell and corresponding line plots as a function of depth for samples of varying heights. (A) Slices of displacement contours underneath migrating cells show significant deformation in the normal direction that decays along the thickness of the sample. Displacement contours are shown for four samples of increasing thickness, ~ 20, 40, 60, 80 µm. The color bar represents the magnitude of the total 3-D displacement vectors (µm), and the cell has been superimposed on the top surface of the sample. The two edges in the image are included to show that there are negligible displacements detected from neighboring cells (contours are dark blue). (B) Corresponding line plots of the total and individual displacement components taken near the leading edges of cells. The x-axis of the plot represents the z-position inside the gel with the origin of the x-axis representing the top surface of the gel.

5.4.4 Analysis of cellular traction forces in 3D: time evolution of force components

Comparing series of confocal stacks affords insight into the time evolution of the displacement and traction profiles produced during cell migration. A planar slice through the top surface of the sample shows how the pattern of displacements changes as a cell moves along the substrate surface (Figure 5-6). The set of images in Figure 5-6 (A) represents 3-D data collapsed into 2-D images, and four successive images of this type are displayed for a 140-minute time course of cell migration. The middle panel of parallel images (Figure 5-6 (B)) shows the total displacements (3-D) of the surface plane as colored contours, while the vectors indicate only in-plane (2-D) displacements. These displacements are then transformed into traction forces in the last panel of complementary images (Figure 5-6 (C)) using the experimentally determined displacement field and material properties.

A polarized cell extending processes in the form of a leading edge generates localized, contractile stresses that change as it propels itself forward (Figure 5-6 (C), 35 min to 70 min). Corresponding retraction forces are observed near the rear of the cell, and corroborate the observation that when cells migrate on substrates of intermediate and high adhesiveness, a portion of their trailing edge can be fractured, leaving behind adhesion receptors (e.g., integrins) on the surface [23, 24]. A similar range of displacement values observed on samples of varying mechanical properties suggests that under typical culturing conditions, cells maintain relatively constant levels of displacement (independent of modulus) within the range of material properties considered here. In accordance with previous studies, the calculated forces on more rigid

Figure 5-6 (A) **Figure 5-6 (B)** **Figure 5-6 (C)**

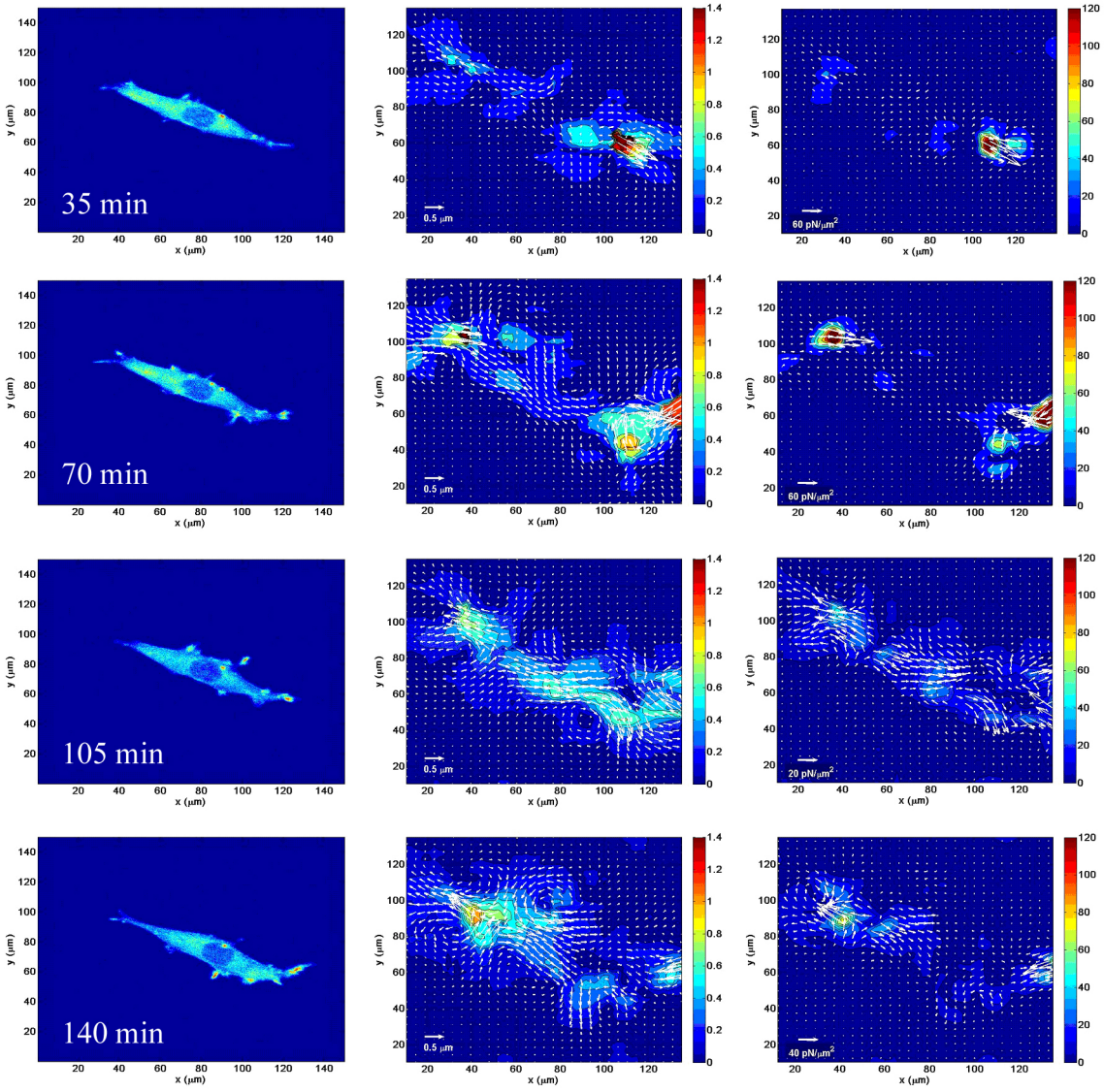

Figure 5-6. Time evolution of displacement and traction force contours during cell migration for a single cell. (A) A series of four successive confocal images recorded during time-lapse imaging experiment. The images shown were captured every 35 minutes for a total of 140 minutes. (B) Consecutive displacement contours and vectors resulting from the motile cell shown in Figure 5-6 (A). The color bar represents the magnitude of the 3-D displacement vectors, and the arrows represent the in-plane displacement vectors. (C) Complementary traction force results calculated directly from displacements in Figure 5-6 (B). The scale bar represents 3-D traction forces in $pN/\mu m^2$, and the arrows represent the in-plane forces.

samples are greater than those on softer ones [25]. Additionally, the regions with the highest traction forces are also the regions with the largest measured displacements. It is important to note that the magnitudes of the forces determined here lie within the range reported for fibroblasts [10, 15], and that these measurements only present the distribution of cellular forces that occur during movement and thus cannot be directly compared to a total detachment force.

At certain time points (e.g., see Figure 5-6 (C): 105–140 min) significant displacements are measurable beneath the cell body near the nucleus, suggesting that a large portion of the cell's contact area participates in force exchange with the substrate. Examination of the contribution of each force component during cell migration showed notable in-plane forces on the ventral surface of the cell that likely indicate frictional forces. Further experiments will be needed to define more clearly the origins of these displacements.

5.4.5 Analysis of cellular traction forces in 3D: "push-pull" phenomena

In many instances, a cell can be seen pulling the matrix from behind while simultaneously pushing a different region of the matrix forward near its leading edge. This new, "push-pull," aspect of cell migration was detected in the normal displacement profiles of monitored cells (Figure 5-7 (A)). 3-D displacement vectors superimposed on displacement contour plots show how this behavior can be seen as the cell deforms the material relative to the surface (Figure 5-7 (B)). The local "pulling" force calculated underneath the rear portion of the cell shown in Figure 5-7 (B) (region I, area ca. 7 μm^2) is approximately 14 nN, and the total force in the entire region (Figure 5-7 (B), region II,

area ca. 16 μm^2) reaches almost 70 nN. Closer inspection of this particular profile at a later time reveals a wave-like pattern in the material (Figure 5-7 (C) and (D)), indicating a coupling of normal and in-plane displacements.

A potential macroscopic analog of this type of 3-D push-pull movement is the rapid surface attachment and detachment of a single seta on a gecko's toe. The toes of these lizards have attracted interest because they can support significant adhesion (normal) and frictional forces (in-plane) that allow the gecko to scale almost any vertical surface [26]. During toe attachment or approach to a surface, individual spatula pads that comprise a seta adhere to the substrate in a near-parallel manner (rolling), followed by gripping of the gecko's toes. In order for the toes to be detached to allow forward movement, a lever-like action pulls the seta upward such that individual spatula pads are peeled from the surface from the rear inward [26]. This peeling mechanism gradually changes the pulling angles between the seta and the surface thereby decreasing the effective van der Waals interaction. Comparing this "rolling and gripping" mechanism of the gecko to the z-displacement patterns observed during cell migration, we find that, subsequent to leading edge extension, the cell must gradually detach its trailing edge in order to move forward. Similar to the lever-action of the gecko, the cell exerts an upward force resulting in an upward displacement to detach the rear.

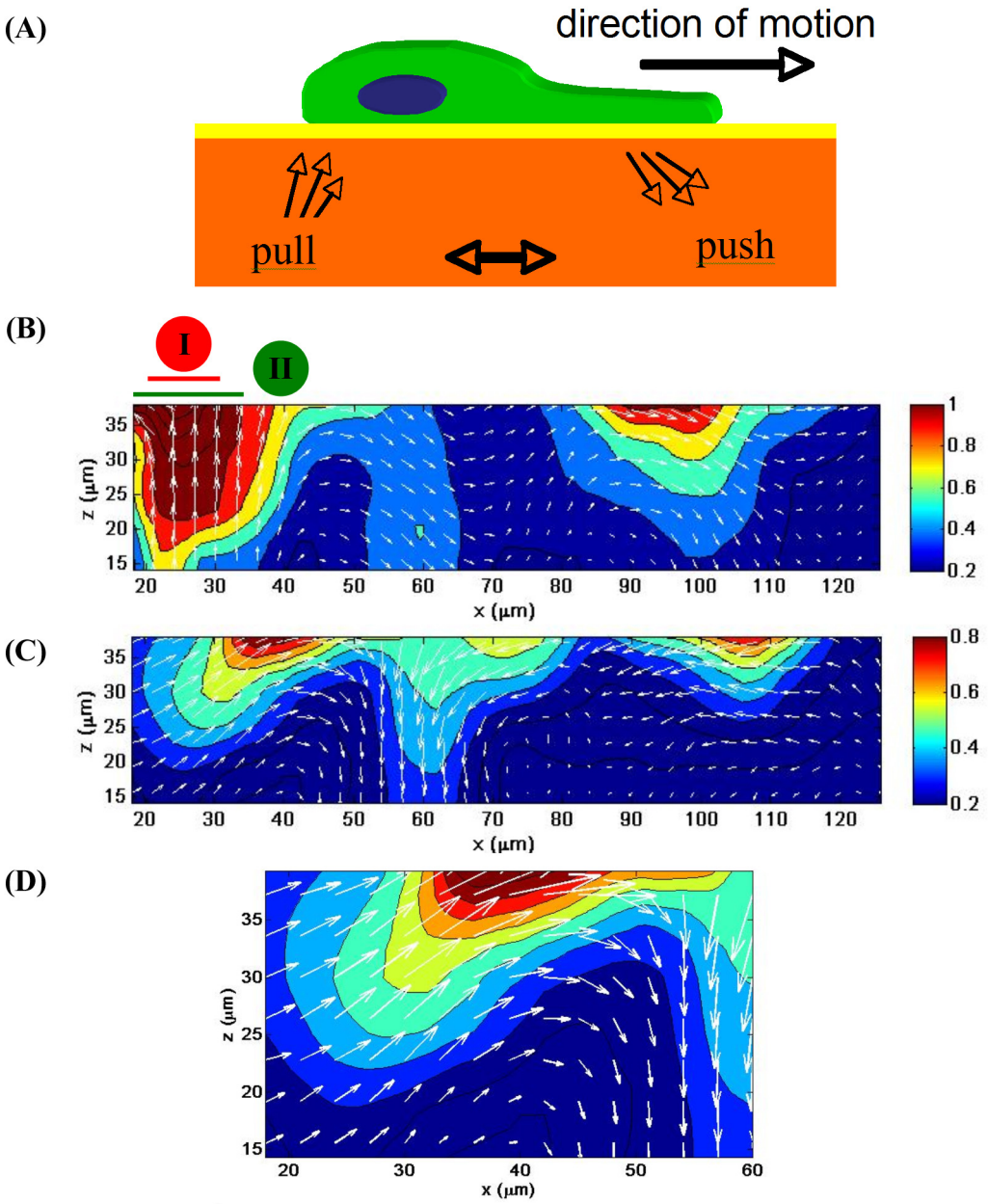

Figure 5-7. 3-D "push-pull" phenomenon observed in the z-plane displacement profiles of tracked cells. (A) Schematic of a cell simultaneously pushing and pulling the underlying material during migration corresponding to a "rolling and gripping" mechanism. (B) The displacement profile in the z-plane illustrates the push-pull hypothesis at t = 35 minutes. A strong pull upwards near the rear of the cell coordinates with the forward motion of the cell and the pushing of the material near the front of the cell. (C) At t = 70 minutes, the change in the displacement pattern shows the dynamic nature of the 3-D "push-pull" mechanism, and a magnified view (D) shows a complex pattern that incorporates both normal and in-plane displacements. The color bar represents the magnitude of the total 3-D displacement vectors, and the arrows represent the displacement vectors in the x-z plane.

5.4.6 Traction force inhibition with blebbistatin

Confirmation of the cellular origins of the measured displacements was accomplished by replicating time-lapse experiments followed by treatment with blebbistatin. Addition of this myosin-II-specific blocker [27] resulted in a gradual inhibition of cell-generated displacements, showing that the localized matrix deformations observed were caused by contraction of actin bundles by myosin-II activity (Figure 5-8).

(A)

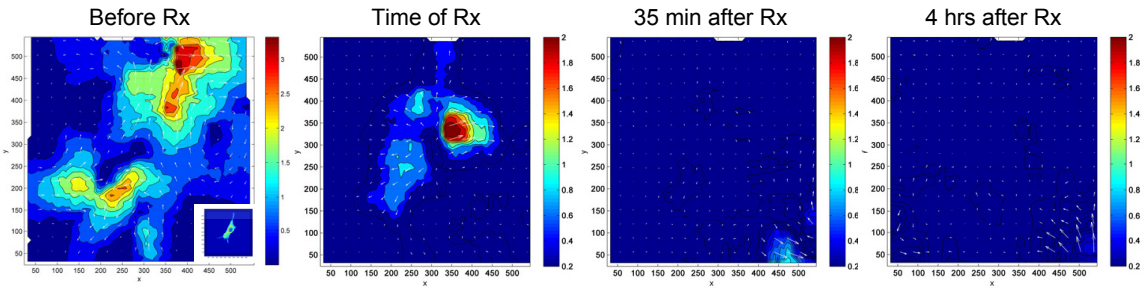

(B)

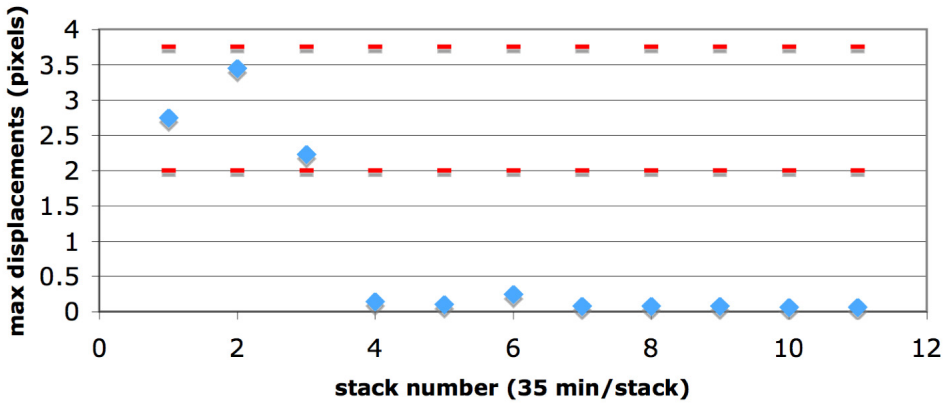

Figure 5-8. Traction force inhibition using blebbistatin: (A) Superimposed planar images of cells and displacement contours before and after treatment (Rx) with blebbistatin; (B) Plot of average maximum displacements measured before and after blebbistatin treatment. Confocal stacks were obtained every 35 minutes.

5.5 Conclusions

This report introduces a new method to track and quantify cellular traction forces in 3-D by using LSCM and DVC. This novel combination of techniques allows dynamic interrogation of the complex process of cell migration and yields further insight into the interactions of cells with their extracellular environments. The approach can be used for local force-mapping of focal adhesions and analysis of the interplay of competing force-fields generated by neighboring cells and sheets of cells. Furthermore, the technique can be extended to elucidate changes in traction forces due to malignant transformation, force profiles of encapsulated cells, and the effect of soluble factors on force production.

5.6 References

1. Discher, D.E., P. Janmey, and Y.L. Wang, *Tissue cells feel and respond to the stiffness of their substrate.* Science, 2005. **310**(5751): 1139-1143.
2. Engler, A.J., et al., *Matrix elasticity directs stem cell lineage specification.* Cell, 2006. **126**(4): 677-689.
3. Zaari, N., et al., *Photopolymerization in microfluidic gradient generators: Microscale control of substrate compliance to manipulate cell response.* Advanced Materials, 2004. **16**(23-24): 2133-2137.
4. Pelham, R.J., and Y.L. Wang, *Cell locomotion and focal adhesions are regulated by substrate flexibility.* Proceedings of the National Academy of Sciences of the United States of America, 1997. **94**(25): 13661-13665.
5. Ingber, D.E., *Mechanobiology and diseases of mechanotransduction.* Annals of Medicine, 2003. **35**(8): 564-577.

6. von Wichert, G., and M.P. Sheetz, *Mechanisms of disease: The biophysical interpretation of the ECM affects physiological and pathophysiological cellular behavior.* Zeitschrift Fur Gastroenterologie, 2005. **43**(12): 1329-1336.

7. Koo, L.Y., et al., *Co-regulation of cell adhesion by nanoscale RGD organization and mechanical stimulus.* Journal of Cell Science, 2002. **115**(7): 1423-1433.

8. Maskarinec, S.A., and D.A. Tirrell, *Protein engineering approaches to biomaterials design.* Current Opinion in Biotechnology, 2005. **16**(4): 422-426.

9. Wang, J.H.C., and J.S. Lin, *Cell traction force and measurement methods.* Biomechanics and Modeling in Mechanobiology, 2007. **6**: 361-371.

10. Dembo, M., and Y.L. Wang, *Stresses at the cell-to-substrate interface during locomotion of fibroblasts.* Biophysical Journal, 1999. **76**(4): 2307-2316.

11. Roy, P., et al., *Microscope-based techniques to study cell adhesion and migration.* Nature Cell Biology, 2002. **4**(4): E91-E96.

12. Tan, J.L., et al., *Cells lying on a bed of microneedles: An approach to isolate mechanical force.* Proceedings of the National Academy of Sciences of the United States of America, 2003. **100**(4): 1484-1489.

13. Galbraith, C.G., K.M. Yamada, and M.P. Sheetz, *The relationship between force and focal complex development.* Journal of Cell Biology, 2002. **159**(4): 695-705.

14. Harris, A.K., P. Wild, and D. Stopak, *Silicone-Rubber Substrata – New Wrinkle in the Study of Cell Locomotion.* Science, 1980. **208**(4440): 177-179.

15. Balaban, N.Q., et al., *Force and focal adhesion assembly: a close relationship studied using elastic micropatterned substrates.* Nature Cell Biology, 2001. **3**(5): 466-472.

16. Franck, C., et al., *Three-dimensional full-field measurements of large deformations in soft materials using confocal microscopy and digital volume correlation.* Experimental Mechanics, 2007. **47**(3): 427-438.

17. Lombardi, M.L., et al., *Traction force microscopy in Dictyostelium reveals distinct roles for myosin II motor and actin-crosslinking activity in polarized cell movement.* Journal of Cell Science, 2007. **120**(9): 1624-1634.

18. Stephens, D.J., and V.J. Allan, *Light microscopy techniques for live cell Imaging.* Science, 2003. **300**(5616): 82-86.

19. Levental, I., P.C. Georges, and P.A. Janmey, *Soft biological materials and their impact on cell function.* Soft Matter, 2007. **3**(3): 299-306.

20. Sabass, B., et al., *High resolution traction force microscopy based on experimental and computational advances.* Biophysical Journal, 2008. **94**: 207-220.

21. Beningo, K.A., et al., *Traction forces of fibroblasts are regulated by the Rho-dependent kinase but not by the myosin light chain kinase.* Archives of Biochemistry and Biophysics, 2006. **456**(2): 224-231.

22. Bhadriraju, K., et al., *Activation of ROCK by RhoA is regulated by cell adhesion, shape, and cytoskeletal tension.* Experimental Cell Research, 2007. **313**: 3616-3623.

23. Palecek, S.P., et al., *Physical and biochemical regulation of integrin release during rear detachment of migrating cells.* Journal of Cell Science, 1998. **111**: 929-940.

24. Cox, E.A., and A. Huttenlocher, *Regulation of integrin-mediated adhesion during cell migration.* Microscopy Research and Technique, 1998. **43**(5): 412-419.

25. Vogel, V., and M. Sheetz, *Local force and geometry sensing regulate cell functions.* Nature Reviews Molecular Cell Biology, 2006. **7**(4): 265-275.

26. Tian, Y., et al., *Adhesion and friction in gecko toe attachment and detachment.* Proceedings of the National Academy of Sciences of the United States of America, 2006. **103**(51): 19320-19325.

27. Kovacs, M., et al., *Mechanism of blebbistatin inhibition of myosin II.* Journal of Biological Chemistry, 2004. **279**(34): 35557-35563.